Journal of Sound and Vibration 326 (2009) 302–313

Contents lists available at ScienceDirect

Journal of Sound and Vibration

journal homepage: www.elsevier.com/locate/jsvi

Experimental characterization of small thickness elastomeric layers submitted to impact loading

Jean-Pierre Arz *, Frédéric Laville

Mechanical Engineering Department, École de Technologie Supérieure, 1100 rue Notre-Dame Ouest, Montréal, Que, Canada H3C 1K3

ARTICLE INFO

Article history:
Received 24 July 2008
Received in revised form
21 April 2009
Accepted 22 April 2009
Handling Editor: C.L. Morfey
Available online 30 May 2009

ABSTRACT

An experimental device has been developed to submit small thickness (<6 mm) elastomeric layer specimens to reproducible impact conditions at high initial impact velocities (1.9–3.8 m s^{-1}). An impulse force test hammer is used as an impactor to measure directly the dynamic force applied on the specimen. As an alternative to classical methods in which position is measured by time integration(s) of accelerometers or velocity sensors, the measurement of the hammer position during impact is achieved by recording its motion with a high-speed camera (at a rate of 30,000 frames per second) and by detecting its position by further analysis on the individual images. Additionally, the initial impact velocity is determined from measurements of the hammer position on the images before contact. The impact model proposed only requires five parameters: two parameters for the impactor (its mass and initial impact velocity) and three parameters for the Hunt–Crossley contact force law describing the specimen. Using a relation issued from the force versus penetration depth diagrams, the estimation of these three contact force parameters can be reduced to the estimation of two independent parameters which roles are well defined and distinct; therefore this estimation can be accomplished with a straightforward trial and error procedure. The method is used to characterize eight impacted elastomeric specimens and is validated with comparisons between experimental and simulation results. These comparisons show that the model is appropriate to simulate with reasonable precision the main experimental characteristics of force and penetration depth signals.

1. Introduction

One way to reduce the sound generated during an impact between two colliding bodies is to reduce the impact force magnitude by adding a soft material layer in the contact zone between the two bodies. Elastomeric materials such as rubber are often used for this interfacing layer. Because of design constraints such as minimal mass and space, the use of a small thickness elastomeric layer is often required in mechanical systems that generate impacts, such as snowmobile tracks, conveyor belts and plastic granulators. Finding the optimal specimen, in terms of material and thickness, has been the motivation to undertake this research on the characterization of impact force for elastomeric layer specimens of small thicknesses.

Among experimental methods for testing rubbers, static indentation is the simplest method to characterize the ability of a material to resist the penetration of an indenter under a specified loading and is notably used to measure the hardness

* Corresponding author.
E-mail address: jean-pierre.arz@etsmtl.ca (J.-P. Arz).

0022-460X/$ - see front matter © 2009 Elsevier Ltd. All rights reserved.
doi:10.1016/j.jsv.2009.04.033

of elastomeric layer specimens (see ISO 48 [1] and ISO 7619 [2]). However, specimens of thickness superior to 6 mm are required and the load applied is low, resulting in small penetration depths into the specimen compared to its thickness. Furthermore, static methods do not take into account the lossy behavior of elastomeric materials, hence dynamic methods have to be used. Vriend and Kren [3] notably proposed a "dynamic indentation method" in order to investigate the viscoelastic properties of elastomeric materials under impact. The experimental method they use consists in an impact device with an indenter attached to a rotating lever. The only variable measured during the impact is the velocity of the indenter, by mean of a stationary inductive coil placed on the specimen and of a permanent magnet mounted on top of the indenter. The contact force and the indenter displacement are determined, respectively, by numerical differentiation and numerical integration of the velocity signal. In this approach, only one material thickness of 6 mm is considered and only one impact velocity ($<1.2\,\mathrm{m\,s^{-1}}$) is tested, leading to small penetration depths compared to the specimen thickness. Another limitation is the use of the linear model of Kelvin–Voigt to describe the behavior of the material because it leads to an unrealistic jump of the force signal values at the beginning of contact, whereas the experimental force time signals are characterized by a continuous increase from zero.

In order to propose a more realistic impact model able to simulate the observed characteristics of our impacted rubber specimens, studies of impact forces achieved in other fields of interest were examined. Based on small elastic strains of two colliding bodies considered as elastic half spaces, Hertz's nonlinear law of contact $F(t)=Ku(t)^{3/2}$ (see [4] for instance), where $u(t)$ represents the relative approach of the impactor and the impacted structure, is certainly the most widely used because K can be easily computed for simple geometries (in particular for sphere–sphere interaction or sphere–plate interaction) in function of the curvature radius and elastic constants (Young modulus and Poisson's coefficient) of both bodies. In several studies, Hertz's contact force is approximated by trigonometric functions in order to simplify the calculations. However, Akay and Latcha showed in [5] that the half-period sinus wave approximation induces unrealistic discontinuities in the acceleration response of the plate during contact whereas the squared half-period sinus wave, by inducing smooth beginning and end of the acceleration response, gives a better approximation of experimental results. A model without this contact force approximation and with the inclusion of a plastic strain phase is presented in [6] to simulate the inelastic impact of a steel sphere on an aluminum plate, but energy losses are still neglected. Many studies of impact force have been found in musical acoustics to simulate percussive instrument sounds because the characteristics of the force (in particular its duration) determine the spectrum of the tone. For simulation of piano sounds, the interaction force between a piano hammer (made of wood and covered with felt) and a piano string has been widely treated in the literature. In order to find the dependencies between the force and the felt compression, several experimental studies used a setup where the piano hammer impacts a force sensor fixed to a rigid surface (see for instance [7,8]). If authors like Chaigne and Askenfelt in [9] started with nonlinear elastic models for their simplicity of use, these models had to be improved to take into account the more complicated experimental characteristics of the felt such as hysteresis and viscoelasticity. One of the latest models (used notably by Bensa, Gipouloux and Kronland-Martinet in [10]) which successfully describes the energy losses and reproduces well the experimental characteristics of the felt is the nonlinear viscoelastic contact force law originally formulated by Hunt and Crossley [11]. Consequently this model used for felt is chosen to test if it can simulate the observed behavior of the elastomeric layer specimens as their dependencies between force and displacements have similar characteristics, the only difference being that the magnitudes of force and penetration depth signals are much larger for the elastomeric specimens than the magnitudes of force and compression signals for the piano hammer felt.

The method used in this paper to characterize the behavior of elastomeric layer specimens under impact includes two steps. The first step, presented in Section 2, is the experimental measurements of the force and the penetration depth into the elastomeric layer specimens under reproducible impact conditions. Details are given on the method developed to measure the penetration depth of the impactor into the specimen from image files of the impactor motion recorded by a high-speed camera; typical experimental curves are also shown to point out their main characteristics. The second step, presented in Section 3, is the use of an appropriate impact model and the extraction of its parameters from the experimental data. Finally, in Section 4, the unique set of contact force parameters for the eight specimens are presented and comparisons between experimental and simulated signals for specimen #1 are shown.

2. Experimental method

2.1. Experimental setup

In order to compare the behavior of different elastomeric layer specimens under various impact conditions, the experimental setup should provide a mean to submit the specimens to reproducible impact conditions (mass m and initial velocity V_0 of the impactor) and a mean to measure during the impact both the impact force and the penetration depth of the impactor into the specimen.

2.1.1. Impact device, force measurement and specimens

The experimental device, presented in Fig. 1, consists in an impact hammer mounted in a rotating lightweight plastic arm to guide its fall towards an elastomeric layer specimen fixed on the vertical face of a massive steel block. A crosshair is

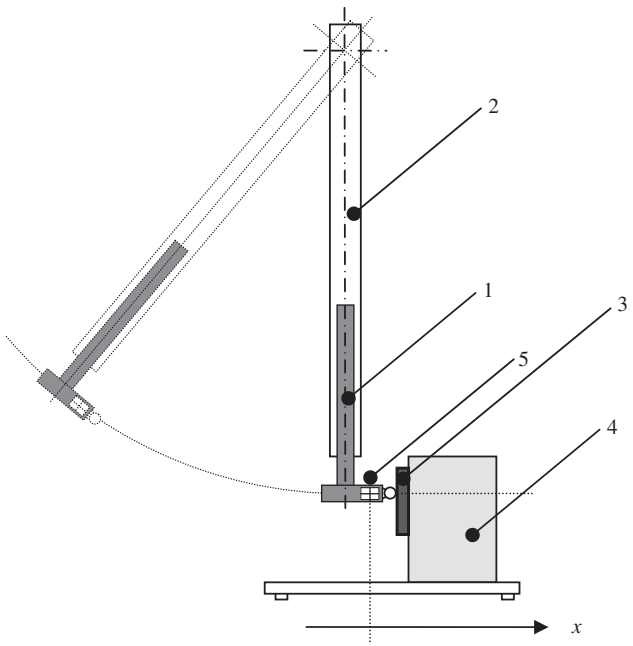

Fig. 1. Scheme of the experimental setup involving: (1) impact hammer; (2) rotating arm; (3) specimen; (4) steel block; and (5) crosshair used for hammer position detection.

Table 1
Characteristics of the eight elastomeric layer specimens tested.

Specimen number	Commercial name	Elastomer type	Shore hardness (HS)	Nominal thickness (mm)	Measured thickness (mm)
1	BNIT	NBR	60	3.175	3.25 ± 0.01
2	NECOM	Neoprene	60	3.175	2.95 ± 0.01
3	SB60	SBR	60	3.175	3.06 ± 0.01
4	PGUM	NR	40	3.175	3.65 ± 0.01
5	BNIT	NBR	60	6.35	5.88 ± 0.01
6	NECOM	Neoprene	60	6.35	6.06 ± 0.01
7	SB60	SBR	60	6.35	5.89 ± 0.01
8	PGUM	NR	40	6.35	6.25 ± 0.01

attached on the hammer head, next to the tip, to facilitate the detection of the hammer position. Comparable devices involving an impactor attached to a rotating arm have been notably developed to have reproducible impact conditions on elastomeric materials [3] and on biological materials like fruits [12]. The height at which the hammer is manually released (with zero initial speed) determines its impact velocity on the specimen and thus enables the experimenter to submit different specimens to reproducible impact velocities. Furthermore, the length of the rotating arm (0.8 m) is large enough firstly to achieve impact velocities of several meters per second and secondly to make the circular trajectory of the hammer approximate a rectilinear horizontal trajectory during impact.

The impactor is an impulse force test hammer (PCB Piezotronics 86C01, sensitivity 11.2 mV/N) integrating an ICP quartz force sensor that converts directly the impact force into electrical signal. In order for the tip to have a well defined geometry and a negligible strain during impact, a steel sphere of 7.9375 mm ($\frac{5}{8}$ in) diameter is attached to the hammer head instead of the regular impact hammer tips. In addition, the resonance frequency of the hammer being higher than 15 kHz, its modal properties can be neglected and it will be considered as a purely inertial element in our models.

The specimens are fixed on a steel block with enough mass and stiffness to make it possible to neglect its displacement and strain during impact. The eight specimens tested, presented in Table 1, involve four different kinds of common elastomeric materials (NBR, Neoprene, SBR and NR). Their shape is a square with 60 mm sides and the only property given by the retailer is their Shore hardness. They were obtained from elastomeric layers of two different nominal thicknesses: 3.175 mm ($\frac{2}{16}$ in) and 6.35 mm ($\frac{4}{16}$ in). However, thickness measurements using a slide caliper showed rather large variations from the nominal thickness from one specimen to the other. The specimen characteristics including their nominal and measured thicknesses are presented in Table 1.

2.1.2. Hammer position measurement using high-speed imaging

In most studies aiming to measure the position of an impactor, the position is actually deduced from measurements of acceleration or velocity by numerical integration. However, some authors like Musiol and Harty in [13] have pointed out the inaccuracy of this numerical integration due to the uncertainty associated with the integration constants (one for a velocity measurement or two for an acceleration measurement). Instead of using an accelerometer or a velocity sensor, the position is obtained by recording the hammer motion during the impact with a high-speed camera and detecting its position by further analysis on the images. The main advantages of this method are: (1) the quantity measured is directly the position of the impactor; (2) it is a non-contact measurement and neither the impactor nor the specimen need additional equipment; (3) once the beginning of contact has been determined, the images before contact can be used to estimate the initial impact velocity of the hammer; and (4) watching the movie at low playback speeds gives further information about the impactor motion (in our tests, it has been noticed that during the loading part of the impact the movement of the hammer head is very close to a pure translation but that during the unloading part there is a deviation from this translation path, probably due to the bending of the arm). The present limitations of the method are its spatial and temporal resolutions. Calibration is performed by taking pictures of a reference length object and by measuring this length in pixel units on the pictures; the result is that one pixel represents a square of about 0.04729 mm side in reality. This spatial resolution could be improved by using a lens having a bigger focal length and the time resolution will certainly be improved in the future when high-speed cameras offer increased frame rates.

2.2. Data acquisition

The hammer motion during impact is recorded by a Photron™ (model FASTCAM-ultima APX) monochrome high-speed camera equipped with a Tamron™ macrolens (model 272E) and an external light source. The axis of the camera is perpendicular to the plan of motion of the hammer and the imaging sensor is located 29 cm away from the impact point. All the acquisition process is handled with the Photron File Viewer™ software application using the followings parameters: (1) number of frames per second: 30,000 fps; (2) shutter "speed": $\frac{1}{120{,}000}$ s, which actually represents the exposition time (the time the light reaches the imaging sensor). To limit blur effects, lower exposition times ($\frac{1}{250{,}000}$ s is the limit of the system) were tested but the pictures obtained were too dark and too noisy to allow precise detection of the hammer position; and (3) resolution of the images: 256×128.

For the impact force data acquisition, the analog voltage given by the force sensor is digitalized by a National Instruments acquisition board (model BNC-2140) controlled by the MATLAB™ Digital Acquisition Toolbox. The same sampling frequency as the one used for the images (30 kHz) is chosen to ease the post-processing by having each time force sample corresponds to an image.

In order to trigger and synchronize the two data acquisition systems used (one for the force, the other one for the camera), an external source delivering an electrical impulse signal to the two systems is manually activated before impact. The data acquired during a test consist of a digitalized temporal force signal and of a movie (.avi) file, both sampled at the same frequency of 30 kHz. The frames of the movie are saved as individual monochrome image (bitmap) files of resolution 256×128. The analysis of these image files in order to detect the position of the hammer is presented in the following section.

2.3. Data processing: penetration depth measurement through image analysis

Since the strains of the steel block and of the hammer tip can be neglected in comparison with the large penetration depths into the rubber specimens, the penetration depth $x(t)-x_0$ is computed from, first, the measurement of the hammer head position $x(t)$ during impact and, second, the determination of the hammer head position x_0 corresponding to the beginning of contact.

2.3.1. Hammer position measurement

The goal of the analysis of the images is to detect with good precision the position of the hammer on each image. To ease the detection, a printed crosshair (made of two thin perpendicular black lines printed on a white background) is attached on the hammer head, next to the tip. The data contained in each (256×128) monochrome image file is a matrix (having 256 columns and 128 lines) of color values in the range 0–255 (8 bits quantification, 0 corresponding to pure black and 255 to pure white).

Since the movement of the hammer during impact is close to a pure horizontal translation, the position detection can be limited to the position of the vertical line along the x-axis. So a horizontal segment is defined on each image and the color values along this segment are plotted; Fig. 2 gives an example of such a plot in dotted line. The black vertical line is characterized by two values lower than 255 (the maximum value). The simplest way to detect the position of the middle of the line would be to find the pixel corresponding to the minimum of color. However, because the size of one pixel is large compared to the width of the line, the real middle of the line can actually be located between two consecutive pixels. To increase the precision of the detection, the color values corresponding to the line are interpolated (one hundred

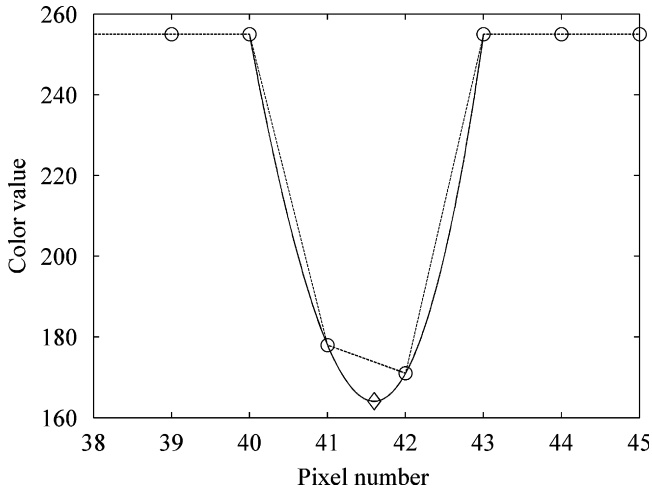

Fig. 2. Detection of the hammer position: effect of the interpolation of color values by a spline fonction: - - o - -: original color values and —: interpolated color values.

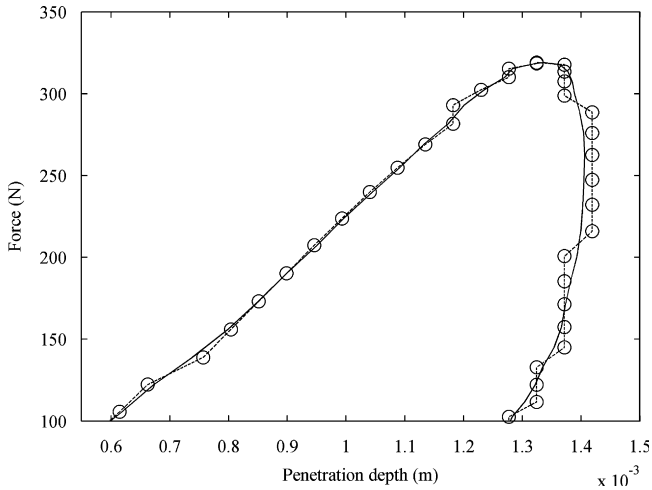

Fig. 3. *F–x* diagram showing the effect of the interpolation of color values on the detected penetration depths during impact: - - o - -: detection based on the raw color values and —: detection based on the interpolated color values.

intermediate values between two consecutive pixels) with a spline function and the minimum color value on this interpolated spline is detected. The interpolated plot is shown with a solid line in Fig. 2.

Additionally, Fig. 3 shows, in the force versus penetration depth representation (this representation will be called the "*F–x* diagram" in what follows), a comparison between the penetrations measured during an impact using the detection based on the raw color values and using the detection based on the interpolated color values. In the case of the raw values detection, the penetration detected for several consecutive frames often stays the same. This is especially noticeable on the part of the curve further to the right, when the penetration is close to the maximum penetration, because the hammer velocity becomes very small. The more precise curves obtained using the interpolated color values are preferred because they lead to a unique maximum penetration value and to a unique corresponding force value, these two values being used in the model parameters estimation procedure presented in Section 3.3. Consequently, all the penetration depth measurements presented hereafter are obtained with the detection based on the interpolated color values.

2.3.2. Detection of the beginning of contact

The beginning of contact is usually determined from the force signal: in theory, it corresponds to the first time sample at which the force is not zero anymore. In practice, the force signal has some noise (and noise level increases for increasing input range) so the determination of the beginning of contact is not very precise. The precision could be increased, firstly by using a higher sampling frequency of the force and, secondly, by using various signal processing techniques. Smoothing techniques have notably been used by Humbert [14] who was able to lower the noise level but found that the determination of the beginning of contact remained arbitrary to some extent.

Alternatively, the beginning of contact could be determined from the position signal by measuring the hammer position when in no load static contact with the specimen and by considering that the dynamic contact occurs at this same position. However, this method leads to non-reproducible results because the dynamic contact does not occur at the exact same location on the specimen so that, due to local thickness variations of the sample, the position corresponding to the beginning of contact will differ from the static case. Consequently, despite the lack of precision, it has been decided to determine the instant $t = 0$ corresponding to the beginning of contact by visual examination of the force signal. The penetration depth is obtained by computing the difference between the position $x(t)$ and the position x_0 at $t = 0$. The complete analysis of the images is performed automatically using MATLAB^{TM} routines.

2.4. Experimental results (for one specimen)

In this section the experimental curves obtained for specimen #1 are presented in Figs. 4 and 5 to point out their main characteristics and choose an appropriate impact model (the experimental results for the seven other specimens have quite similar characteristics).

Fig. 4 shows the nine curves of force versus penetration depth obtained for three different impact velocities and three trials for each velocity; the main characteristics are: (1) hysteresis is important (loading and unloading paths are different); (2) dependencies between force and penetration depth are nonlinear, both for the loading and the unloading paths; and (3) the slope of the loading path tends to increase with increasing velocity, so the specimen also exhibit viscous behavior.

The same experimental force and penetration depth signals as the ones presented in Fig. 4 are plotted in Fig. 5 as a function of time. For clarity, three separate graphics (a), (b) and (c) corresponding, respectively, to impact velocities of 1.93, 2.98 and 3.78 m s^{-1} are presented and each graphic shows three trials for one velocity. The main observations are : (1) the maximum penetration depth occurs later than the maximum force, which is characteristic of the viscoelastic behavior; (2) the contact time tends to decrease with increasing V_0, which is characteristic of the nonlinear behavior; and (3) at the end of the contact (when F reaches 0), there is some residual strain of the specimen. For some specimens, this residual strain is completely recovered after a certain period of time after the impact but, for other specimens, at least a part of the strain is never recovered and corresponds to a clearly visible permanent indentation into the specimens.

As mentioned in the introduction, the experimental dependencies between impact force and penetration depth signals found in our rubber characterization tests turn out to be comparable to the ones available in the literature for the piano hammer felt tests in compression (see examples of F–x curves in [8] for instance), the only difference being the greater magnitudes of force and displacement signals in our case. Consequently, it has been decided to test if the model used for the piano hammer felt could simulate the observed behavior of elastomeric layer specimens under impact.

3. Impact model and estimation of parameters

3.1. Impact model equations

The impact model is described by a system of two equations in the time domain:

$$\sum \text{Forces} = F(x, \dot{x}) = -m\ddot{x}, \tag{1}$$

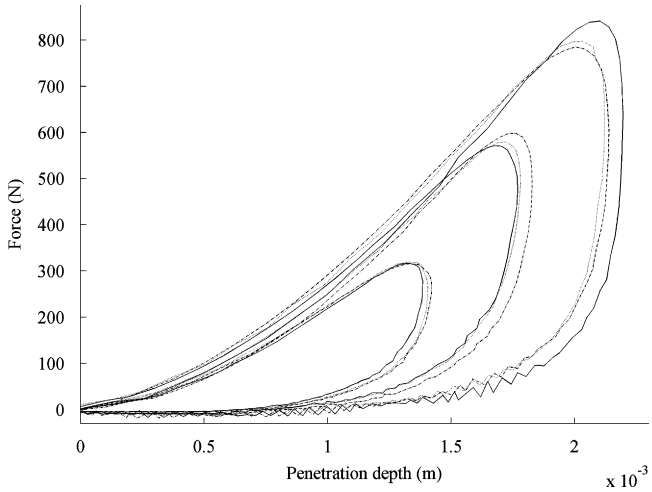

Fig. 4. Experimental F–x diagrams for three different initial impact velocities ($V_1 = 1.93$ m s^{-1}, $V_2 = 2.98$ m s^{-1} and $V_3 = 3.78$ m s^{-1} from inner to outer loops) on specimen #1. Three trials are presented for each impact velocity.

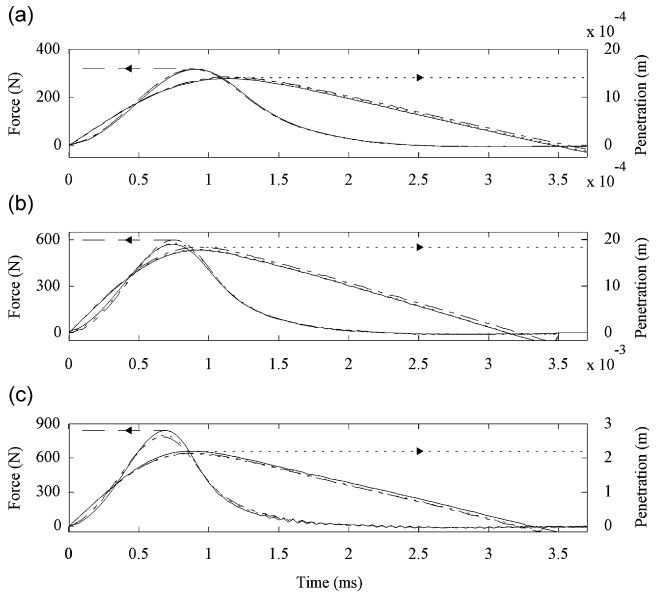

Fig. 5. Experimental force and penetration depth time signals for three different initial impact velocities on specimen #1. Three trials are presented for each impact velocity: (a) $V_1 = 1.93\,\mathrm{m\,s^{-1}}$; (b) $V_2 = 2.98\,\mathrm{m\,s^{-1}}$; and (c) $V_3 = 3.78\,\mathrm{m\,s^{-1}}$. Force values are displayed on the left axis, penetration depth values are displayed on the right axis.

$$F(x,\dot{x}) = kx^{\alpha}(1+\mu\dot{x}). \tag{2}$$

Eq. (1) is Newton's second law applied to the impact hammer considered as a non-vibrating punctual mass m in translation along a horizontal x-axis. In reality, vibrations of the hammer can be observed in the rapid fluctuations variations of $F(t)$ at the end of the unloading part (especially for the higher impact velocity tested, see Figs. 4 and 5(c) for instance) but their amplitude is rather small.

Eq. (2) is the nonlinear viscoelastic contact force law originally formulated by Hunt and Crossley which has notably been used by Marhefka and Orin in [15] to simulate impacts on robotic systems and by Bensa and al. in [10] to model the felt compression of a piano hammer. The contact force is the sum of an elastic term kx^{α} and a dissipative term $\mu k x^{\alpha}\dot{x}$. Because the dissipative term is proportional to the product $x^{\alpha}\dot{x}$, its value is zero at $t = 0$, which constitutes an advantage compared to the more classical Kelvin-Voigt model leading to non-realistic positive values of $F(t)$ at $t = 0$.

3.2. Numerical resolution

To solve the system of Eqs (1) and (2), the quantities $F(t)$, $x(t)$, $\dot{x}(t)$ and $\ddot{x}(t)$ must be evaluated at discrete instants $t = n \times \Delta t$ with $n = [0, 1, 2, \ldots, N]$, N corresponding to the end of contact. The shorter notation $U_n = U(n \times \Delta t)$ is adopted. The resolution in this simple case of impact on a rigid structure is straightforward using standard explicit differences schemes: by choosing to approximate the speed $\dot{x}(t)$ with a first order decentered operator $\dot{x}_n = 1/\Delta t(x_n - x_{n-1}) + o(\Delta t)$ and the acceleration $\ddot{x}(t)$ with a second order centered operator $\ddot{x}_n = 1/(\Delta t)^2(x_{n-1} - 2x_n + x_{n+1}) + o(\Delta t)^2$, the system can be explicitly solved at each time step using a loop:

for $n = 1{:}N$,

$$F_n = kx_n^{\alpha}\left(1 + \mu\frac{x_n - x_{n-1}}{\Delta t}\right)$$

$$x_{n+1} = \frac{-\Delta t^2}{m}F_n + 2x_n - x_{n-1}$$

end,

with the following initial conditions:

- at $t = 0$, $x_0 = 0$ and $F_0 = 0$,
- at $t = \Delta t$, $x_1 = V_0 \times \Delta t$.

3.3. Estimation of parameters

A total of five physical parameters have to be given to the model: the mass m of the impactor, its initial impact velocity V_0 and the three parameters (α, μ, k) of the contact force law.

The value of m represents the effective mass of the impacting device and is a constant for all the tests: $m = 0.1$ kg. The impact velocity V_0 is experimentally determined for each test by detecting the hammer position on the 10th frame before the beginning of contact (with the same method of interpolation of the color signal as the one previously presented and used during contact) and by calculating the velocity with:

$$V_0 = \frac{x_{-10} - x_0}{10\Delta t}, \tag{3}$$

where x_{-10} represents the hammer position on the 10th frame before contact and x_0 the position at the beginning of contact.

The general method used to evaluate the three parameters (α, μ, k) of the contact force is based on comparisons between simulation and experimental signals of force and penetration depth. From observations on F–x diagrams, a relation between α and k is derived using the fact that at the maximum penetration depth (which corresponds to the point at the extreme right of the plot) the velocity is zero. Expressing Eq. (2) at this point gives

$$F(x_{\max}, 0) = kx_{\max}^{\alpha}. \tag{4}$$

Because of this relation, the number of independent parameters to be estimated reduces from three to two. The two parameters α and μ have been chosen as unknown variables and a trial and error procedure was used to estimate their best values. The estimation is fairly straightforward because the roles of α and μ are well defined and distinct: the three curves of Fig. 6 illustrate that the effect of α is to control the curvature of the F–x curve and the three curves of Fig. 7 illustrate that the effect of μ is to control the hysteresis (the "width" of the F–x loop).

4. Results

This section is divided into three subsections: first, the variability of experimental data is discussed; second, the method used to characterize each specimen by unique parameters (α, k, μ) of the force law is described; and third, the unique parameters (α, k, μ) estimated for each specimen are given in Table 3 and comparisons between simulation and experimental data for specimen #1 are presented in Figs. 8 and 9.

4.1. Variability of experimental data

In order to judge for the variability of experimental data, Figs. 8 and 9 show for specimen #1 three trials for each impact velocity tested ($V_1 = 1.93\,\mathrm{m\,s^{-1}}$, $V_2 = 2.98\,\mathrm{m\,s^{-1}}$ and $V_3 = 3.78\,\mathrm{m\,s^{-1}}$). For each impact velocity, some variability of the experimental maxima values of force and penetration depth can be observed. To check if the variability in impact velocity could explain the observed variation in the experimental maxima of force and penetration depth, a simulation was conducted using the individual impact velocity measured for each test. The simulation curves presented in Fig. 8 show less variations than the experimental results, therefore the variability of impact velocities do not explain the experimental

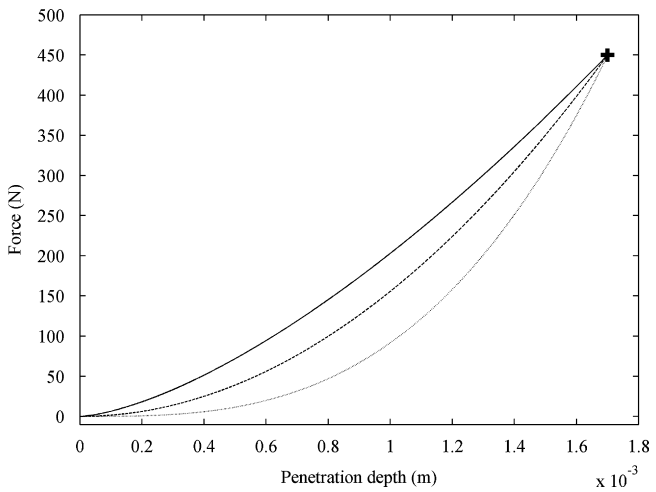

Fig. 6. Role of parameter α: F–x diagram for $m = 0.1$ kg, $V_0 = 3\,\mathrm{m\,s^{-1}}$, $\mu = 0$ and three values of α: —: $\alpha = \frac{3}{2}$; - - -:$\alpha = 2$; and …: $\alpha = 3$. Each curve passes by the point of coordinates (1.7e−3 m, 450 N).

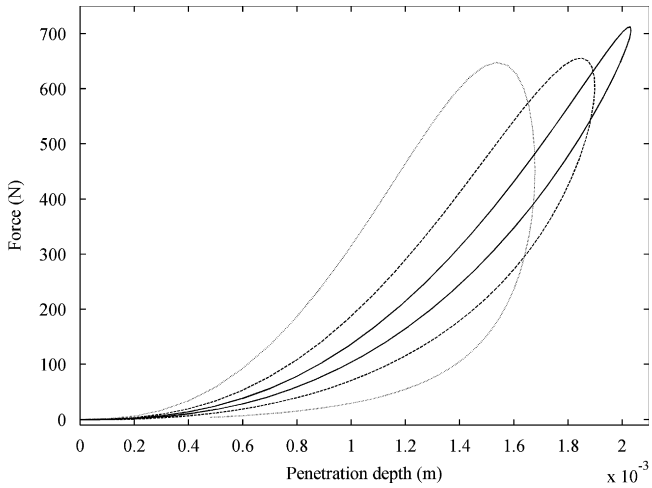

Fig. 7. Role of parameter μ: F–x diagram for $m = 0.1$ kg, $V_0 = 3\,\mathrm{m\,s^{-1}}$, $\alpha = 2.5$, $k = 3.776 \times 10^9\,\mathrm{N\,m^{-\alpha}}$ and three values of μ: —: $\mu = 0.05$; - - -: $\mu = 0.2$; and …: $\mu = 0.6$.

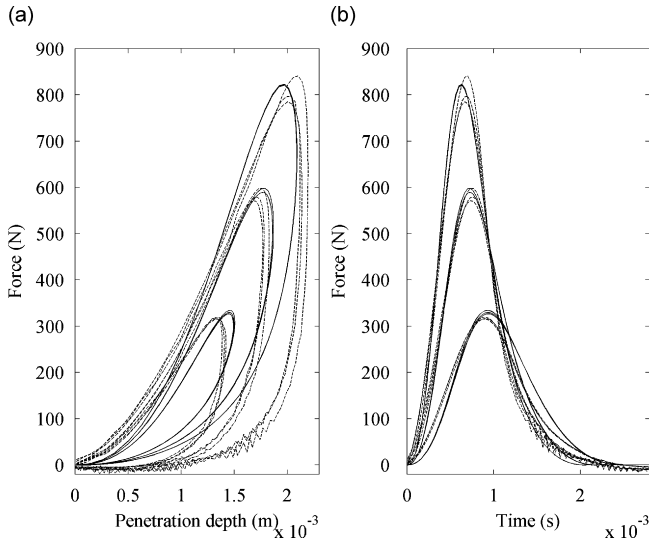

Fig. 8. Specimen #1: comparisons between measurements and simulations for the nine trials: (a) F–x diagram and (b) force versus time. ----: measurements and —: simulations.

variability (this is not too surprising because the experimental setup was designed to achieve reproducible impact velocities). In fact, the velocity standard deviation calculated on 24 trials at each of the three release heights never exceeds 3 percent.

Because the experimental variability is not due the variability of impact velocities, two other explanations can be proposed. First, variations of $x_{\max}$ may be due to the incertitude in defining the beginning of contact. This problem has also been noticed by Humbert [14] in experimental measurements of the felt compression of a piano hammer under impact. More precisely, the inaccuracy in determining the beginning of contact from the force signal results in a translation of the curves along the x-axis. Second, the variations of $F_{\max}$ can be explained by local variations of the specimen thickness and also by its heterogeneous composition (clearly seen by eye) that may result in local variations of its physical properties.

4.2. *Unique parameters* (α, k, μ)

The trial and error procedure presented in Section 3.3 to evaluate the parameters (α, k, μ) of a specimen could be applied individually to each test, leading to different values of these parameters for each test. However, an important attempt of the characterization is to describe the specimen with unique parameters (α, k, μ) and to test the ability of the model to simulate its behavior over a large range of impact velocities with these unique parameters. In order to do so, the trial and error

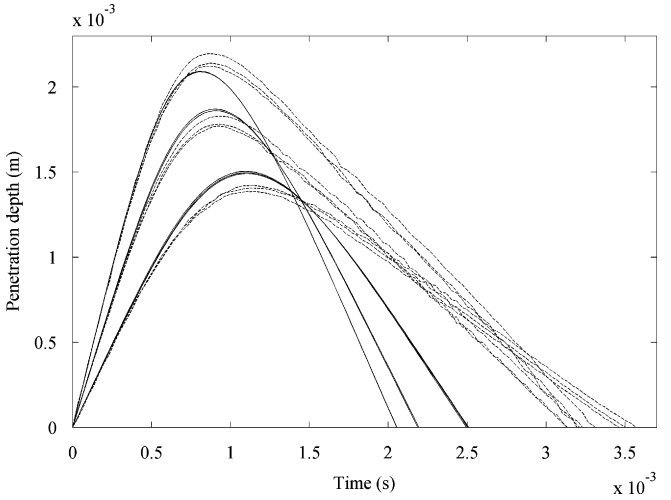

Fig. 9. Specimen #1: time domain comparisons between measurements and simulations of penetration depth for the nine trials. ----: measurements and —: simulations.

Table 2
Variations of experimental parameter k for the eight specimens. $\overline{k_{v_1}}$, $\overline{k_{v_2}}$ and $\overline{k_{v_3}}$ are the means of k over the three trials at respective impact velocities $V_1 = 1.93\,\mathrm{m\,s^{-1}}$, $V_2 = 2.98\,\mathrm{m\,s^{-1}}$ and $V_3 = 3.78\,\mathrm{m\,s^{-1}}$.

Specimen number	$\overline{k_{v_1}}$	$\overline{k_{v_2}}$	$\overline{k_{v_3}}$	$\overline{k_v}$	$\pm\sigma_{k_v}$ (%)
1	9.740E+08	1.005E+09	8.507E+08	9.432E+08	±7.97
2	2.851E+09	4.286E+09	3.808E+09	3.648E+09	±17.84
3	9.909E+08	9.402E+08	8.120E+08	9.143E+08	±11.21
4	4.231E+17	4.860E+17	5.722E+17	4.938E+17	±14.26
5	2.030E+07	2.077E+07	2.061E+07	2.056E+07	±4.89
6	1.909E+07	1.887E+07	1.890E+07	1.896E+07	±3.42
7	9.581E+07	8.816E+07	1.004E+08	9.478E+07	±10.31
8	3.727E+09	3.045E+09	3.178E+09	3.316E+09	±9.94

$\overline{k_v}$ and σ_k are the mean and standard deviation of k over the nine trials on each specimen.

procedure is used with the following specificities: a unique α value is chosen for the nine trials, an individual k parameter is calculated for each trial and a unique μ value is chosen for the nine trials. Doing so, k is the only parameter having variations and Table 2 shows for each specimen the mean values ($\overline{k_{v_i}}$) of k over three trials for each impact velocity ($i = 1, 2, 3$) and the mean and standard deviation values ($\overline{k_v}$ and σ_{k_v}) of k over the nine trials for a specimen. No particular relation between impact velocities and $\overline{k_{v_i}}$ values exist, therefore $\overline{k_v}$, the mean value of $\overline{k_{v_i}}$ over the three impact velocities, can be chosen as the unique value of the parameter k. The table shows a fairly high standard deviation for k (up to 17.8 percent for specimen #2) which can be explained by the experimental variability of $x_{\max}$ and $F_{\max}$ values mentioned in Section 4.1.

4.3. Comparisons between simulation and experimental data

Comparisons between simulation and experimental data are presented for specimen #1 in Figs. 8 and 9. In Fig. 8, F versus x plots are shown in one window and F versus time plots are shown in another window. The experimental data for the nine tests (three impact velocities and three trials for each velocity) are presented in dashed line and the nine corresponding simulation results are presented in solid line. The values of the parameters used for the simulations are $m = 0.1$ kg and (α, k, μ) as defined in Table 3, so only the impact velocity V_0 parameter is given an individual experimental value for each trial.

A general remark from Fig. 8 is that the experimental force versus time signals are well predicted but that the predictions are less accurate in the F–x representation, especially for the unloading part of the process. This is confirmed by the penetration depth versus time plots, shown in Fig. 9: the loading part of the penetration is well predicted but, for the unloading part, the predicted penetration is smaller than the experimental penetration.

The three materials of hardness 60 HS (specimens 1–3 and 5–7) are characterized by different values of α and by identical values of μ for one thickness; their global behavior is quite comparable in terms of force and penetration depth ranges. The fourth material (specimens 4 and 8) is characterized by higher values of α and smaller values of μ.

Table 3
Contact force parameters values for the eight elastomeric layer specimens.

Specimen number	α	$\overline{k_v}(Nm^{-\alpha})$	$\mu\,(s\,m^{-1})$
1	2.3	9.432E+08	0.3
2	2.5	3.648E+09	0.3
3	2.2	9.143E+08	0.3
4	6	4.938E+17	0.1
5	1.8	2.056E+07	0.25
6	1.8	1.896E+07	0.25
7	2	9.478E+07	0.25
8	3	3.316E+09	0.05

When comparing the two thicknesses for one material, it turns out that the α parameter decreases as thickness increases and stays always higher than the Hertz's law limiting value of $\frac{3}{2}$. This limiting value is expected to be reached in the case of large thickness specimens that would verify the assumption of an "infinite half space".

5. Conclusion and recommendations

An experimental device was developed to produce impacts on elastomeric specimens with highly reproducible initial velocities (from 1.9 to 3.8 $m\,s^{-1}$). A non-contact measurement of the penetration depth into the specimens is performed using a high-speed imaging technique which measures directly the position of the impactor (no need for time integration) with good spatial and time resolutions. Additionally, this measurement technique gives the initial impact velocity and offers the possibility of watching the impactor motion at low playback speeds. Using this experimental characterization method, eight elastomeric specimens (four materials and two thicknesses) have been tested and the main experimental characteristics (hysteresis, nonlinear force-penetration depth laws and viscoelasticity) were successfully reproduced using an impact model simulation. The impact model requires a total of five parameters: two for the impactor (mass and velocity) and the three parameters of the Hunt–Crossley contact force law which describes the specimen. When extracting these contact force parameters from a set of trials at different velocities, it was found that each specimen could be characterized by a unique set of parameters over the whole range of impact velocities.

This model could be improved in two ways. First, to better predict the unloading part of the impact, a more elaborate model could be developed to take into account the possible residual strain of the specimen, including recoverable and non-recoverable parts. Second, to better account for the effect of the specimen thickness, this parameter could be included in the contact force law. Other tests involving bigger and smaller thicknesses would be required.

As the ultimate goal of this study is noise and vibration reduction, the present contact model can be used in two different cases: in the case of an existing mechanism (in which colliding structures produce a known vibration and noise level) and in the case of a mechanism at the design stage. In the first case, the impact force reduction prediction is used to predict the vibration and noise reduction when an elastomeric layer is added in the contact zone (as there is a linear relationship between the force and the resulting vibration and noise). In the second case, the impact force model needs to be complemented with a vibration and radiation model of the structure in order to evaluate the influence of the layer parameters on the vibrations and the radiated sound of the colliding structures.

Acknowledgment

The authors gratefully acknowledge the support of NSERC (Natural Sciences and Engineering Research Council of Canada).

References

[1] International Organization for Standardization ISO 48, Physical testing of rubber, methods for the determination of hardness, 1994.
[2] International Organization for Standardization ISO 7619, Rubber-determination of indentation hardness by means of pocket hardness meters, 1997.
[3] N.M. Vriend, A.P. Kren, Determination of the viscoelastic properties of elastomeric materials by the dynamic indentation method, *Polymer Testing* 23 (4) (2004) 369–375.
[4] W. Goldsmith, *Impact: The Theory and Physical Behaviour of Colliding Solids*, Edward Arnold, London, 1960.
[5] A. Akay, M. Latcha, Sound radiation from an impact-excited clamped plate in an infinite baffle, *Journal of the Acoustical Society of America* 74 (2) (1983) 640–648.
[6] P. Trocaz, R. Woodcock, F. Laville, Acoustic radiation due to the inelastic impact of a sphere on a rectangular plate, *Journal of the Acoustical Society of America* 108 (5 Pt. 1) (2000) 2197–2202.
[7] N. Giordano, J.P. Winans Ii, Piano hammers and their force compression characteristics: does a power law make sense, *Journal of the Acoustical Society of America* 107 (4) (2000) 2248–2255.
[8] A. Stulov, Hysteretic model of the grand piano hammer felt, *Journal of the Acoustical Society of America* 97 (4) (1994) 2577–2585.

[9] A. Chaigne, A. Askenfelt, Numerical simulations of piano strings. I. A physical model for a struck string using finite element methods, *Journal of the Acoustical Society of America* 92 (2) (1994) 1112–1118.
[10] J. Bensa, O. Gipouloux, R. Kronland-Martinet, Parameter fitting for piano sound synthesis by physical modeling, *Journal of the Acoustical Society of America* 118 (1) (2005) 10.
[11] K.H. Hunt, F.R.E. Crossley, Coefficient of restitution interpreted as damping in vibroimpact, *Journal of Applied Mechanics* 42 (2) (1975) 440–445.
[12] M. Van Zeebroeck, E. Tijskens, P.V. Liedekerke, V. Deli, J.D. Baerdemaeker, H. Ramon, Determination of the dynamical behaviour of biological materials during impact using a pendulum device, *Journal of Sound and Vibration* 266 (3) (2003) 465–480.
[13] C. Musiol, D. Harty, *The Use of Numerical Integration for the Estimation of Displacement from an Accelerometer Signal*, *Application Note*, Vol. 12, nCode International Ltd., 1991.
[14] E. Humbert, *Experimental Study and Numerical Simulation of the Piano-String Interaction for Real-Time Synthesis*, DEA ATIAM and IRCAM, Paris, 2002 (in French).
[15] D.W. Marhefka, D.E. Orin, A compliant contact model with nonlinear damping for simulation of robotic systems, *IEEE Transactions on Systems, Man, and Cybernetics—Part A: Systems and Humans* 29 (6) (1999) 566–572.